LIMNOLOGY
and
OCEANOGRAPHY: METHODS

Limnol. Oceanogr.: Methods 9, 2011, 1–13

Measurement and interpretation of solute concentration gradients in the benthic boundary layer

Moritz Holtappels[1], Marcel M.M. Kuypers[1], Michael Schlüter[2], and Volker Brüchert[1,3]*
[1]Max Planck Institute for Marine Microbiology, Celsiusstrasse 1, 28359 Bremen
[2]Alfred Wegener Institute for Polar and Marine Research, Am Handelshafen 12, 27570 Bremerhaven
[3]Department of Geological Science, Stockholm University, 10691 Stockholm, Sweden

Abstract

The coastal ocean is characterized by high exchange rates of organic matter, oxygen, and nutrients between the sediment and the water column. The solutes that are exchanged between the sediment and the overlying water column are transported across the benthic boundary layer (BBL) by means of turbulent diffusion. Thus, solute concentration gradients in the BBL contain valuable information about the respective fluxes. In this study, we present the instrumentation and sampling strategies to measure oxygen and nutrient concentration gradients in the BBL. We provide the theoretical background and the calculation procedure to derive ratios of nutrient and oxygen fluxes from these concentration gradients. The noninvasive approach is illustrated at two sampling sites in the western Baltic Sea where nutrient and oxygen concentration gradients of up to 5 and 30 μM m^{-1}, respectively, were measured. Nutrient and oxygen flux ratios were used to establish a nitrogen flux balance between sediment and water column indicating that 20% and 50% of the mineralized nitrogen left the sediment in form of N_2 (station A and B, respectively). The results are supported by sediment incubation experiments of intact sediment cores, measuring denitrification rates, and oxygen uptake. The presented flux ratio approach is applicable without knowledge of turbulent diffusivities in the BBL and is, therefore, unaffected by non–steady-state current velocities and diffusivities.

The sediments of coastal waters play an important role in the degradation of organic matter and the subsequent regeneration of nutrients, which are necessary to sustain primary production in the surface waters. Coastal and shelf sediments receive 25–50% of the primary production from the photic zone (Wollast 1991). More than 90% of carbon, nitrogen, and phosphorus bound to deposited organic material that reaches the sediment surface is mineralized and released to the overlying water column to fuel new primary production (Berner 1982). This leads to a tight temporal and spatial coupling of sedimentary and water column processes (Graf 1992; Graf et al. 1995; Soetaert et al. 2000). Hence, a qualitative and quantitative description of organic matter mineralization and nutrient exchange across the sediment–water interface is required to understand the carbon and nutrient cycling in the ocean.

Mineralization processes in the sediment and transport of solutes across the sediment-water interface have been studied using a diversity of approaches, all with different advantages and drawbacks. Well established is the measurement of vertical chemical gradients in the sediment, using microsensors (Jørgensen and Revsbech 1985), optodes (Wenzhoefer et al. 2001), and porewater analysis (Schulz 2000). However, this gradient-diffusion approach does not consider the convective solute flux caused by burrowing fauna in the sediment (i.e., bioirrigation) that can considerably exceed the diffusive flux (Glud et al. 1994). Alternatively, solute fluxes across the sediment–water interface are determined experimentally using closed chambers to incubate sediment samples and the overlying water (Glud et al. 1995). The flux due to bioirrigation is taken into account when the incubated sediment area is large enough to represent the average diversity and abundance of the sediment fauna. A drawback of the incubation approach is that the closed system changes the environmental conditions,

*Corresponding author: E-mail: mholtapp@mpi-bremen.de

Acknowledgment

We thank Bernd Schneider and Anne Loeffler (Leibniz Institute for Baltic Sea Research, Warnemünde) who provided ship time on RV *Professor Albrecht Penck*; Gaute Lavik for assistance in mass spectrometry and data analysis, G. Klockgether, M. Meyer, and J. Schmidt for analytical assistance, F. Wenzhoefer, H. Roy, and P. Faerber for technical assistance and the crews of RV *Heinke* and RV *Professor Albrecht Penck* for excellent collaboration. This study was funded through DFG-Research Center/Excellence Cluster, "The Ocean in the Earth System," and the Max Planck Society.

DOI 10.4319/lom.2011.9.1

especially the bottom water flow (Tengberg et al. 2005). The incubated water needs to be mixed artificially to simulate the flow of the bottom water. However, the degree of stirring can change the concentration of suspended particulate matter, the behavior of the macrofauna, or the porewater flow in permeable sediments.

In recent years increasing attention has been paid to the water layer just above the sediment—the so called benthic boundary layer (BBL)—which is characterized by turbulent boundary layer flow (Dade et al. 2001). As this layer intimately links the sediment to the water column, it is well-suited for the noninvasive observation and quantification of concentration gradients and fluxes between sediment and water column. So far, only a few studies (Ritzrau 1996; Thomsen and Graf 1994) on particle and solute concentrations in the BBL are published. However, none of these studies quantified the exchange of solutes between sediment and water column. A new approach that allows estimating fluxes in the turbulent boundary layer is the eddy correlation technique. Kawanisi and Yokosi (1997) were the first to use the eddy correlation technique to determine the flux of suspended sediment in a boundary layer, whereas Berg et al. (2003) recently introduced this technique to aquatic science to determine oxygen fluxes. The eddy correlation technique measures the instantaneous flux in the turbulent flow field above the sediment. It requires the simultaneous measurement of flow velocities and solute concentrations at high temporal and spatial resolution. To date, only oxygen micro-sensors fulfill these requirements. Currently, the eddy correlation technique cannot be applied to measure the flux of solutes such as nutrients, CO_2, CH_4, and N_2, because no suitable sensors are available for these compounds.

In the following, we present new instrumentation and sampling strategies for the successful measurement of nutrient and oxygen concentration gradients in the BBL. We introduce the theoretical background to calculate relative nutrient and oxygen fluxes from these concentration gradients. We describe the measurement of concentration gradients and the calculation of relative nutrient and oxygen fluxes at two sampling sites in the western Baltic Sea. We illustrate the potential of this approach by establishing a complete nitrogen flux balance between the sediment and the water column. Advantages and limitations of this new approach are discussed thereafter.

Materials and procedures

Theoretical considerations

Vertical mass transport across the BBL changes from molecular diffusion to turbulent mixing with increasing distance from the sediment. The random nature of turbulent flow allows describing the mixing of solutes as a quasi diffusive transport according to Fick's first law of diffusion:

$$J = -D_T \frac{\partial C}{\partial z} \tag{1}$$

where J denotes the flux, D_T is the turbulent diffusivity, and $\partial C/\partial z$ is the vertical concentration gradient of a solute. The turbulent diffusivity is a property of the turbulent flow field, and thus, varies with current velocity, density stratification, and bottom roughness. The logarithmic Law of the Wall (log-law) (von Kármán 1930) provides a link between the average current velocity in a boundary layer and the turbulent diffusivity therein. Assuming a homogeneous bottom roughness (z_0) and steady-state flow conditions, it states that the average current velocity ($\bar{U}$) increases logarithmically with distance (z) from the sediment (Fig. 1A):

$$\bar{U}(z) = \frac{u_*}{\kappa} \ln\left(\frac{z}{z_0}\right) \tag{2}$$

with the von Kármáns constant κ (~0.41) and the friction velocity u. The log-law was experimentally validated in several flume experiments (some reviewed in Pope 2000). Assuming that the turbulent viscosity equals the turbulent diffusivity, the turbulent diffusivity D_T is given by (Tennekes and Lumley 1972):

$$D_T(z) = u_* \kappa z \tag{3}$$

For a stationary current velocity profile $\bar{U}$, the friction velocity u_* is constant, and the turbulent diffusivity increases linearly with distance from the sediment (Fig. 1B). To describe the solute transport across the BBL, we assume a steady-state flux across the sediment–water interface and that the rates in the BBL do not contribute significantly to the flux across the BBL. Substituting Eq. 3 into Eq. 1, we can solve for the concentration gradient. Subsequent integration leads to the following equation for the concentration profile:

$$C(z) = -\frac{J}{u_* \kappa} \ln\left(\frac{z}{z_1}\right) + C_1 \tag{4}$$

with the concentration C_1 at $z = z_1$. For a steady state flux across the BBL, the solute concentration changes logarithmically with distance from the sediment. The steepest gradients are found close to the sediment where the turbulent diffusivity is low (Fig. 1C + D).

The log-law and the related Eqs. 3 and 4 give a first impression of how the concentration gradients in the BBL are tied to the flow field. However, the applicability of the log-law in natural environments is problematic (Lorke et al. 2002; Holtappels and Lorke 2010). Boundary layer flows in oceans and lakes can differ from those in laboratory flumes as they may exhibit density stratification and nonstationary flow that result in nonlinear behavior of D_T (such as the gray dashed profile in Fig. 1B). Here, the log-law and its derivatives serve as a first approximation, from which we assume that turbulent diffusivities are decreased close to the sediment, causing increased concentration gradients. The sampling for detectable concentration gradients should, therefore, focus on the lower part of the turbulent BBL (Fig. 1 C + D). The direction of the concentration gradient

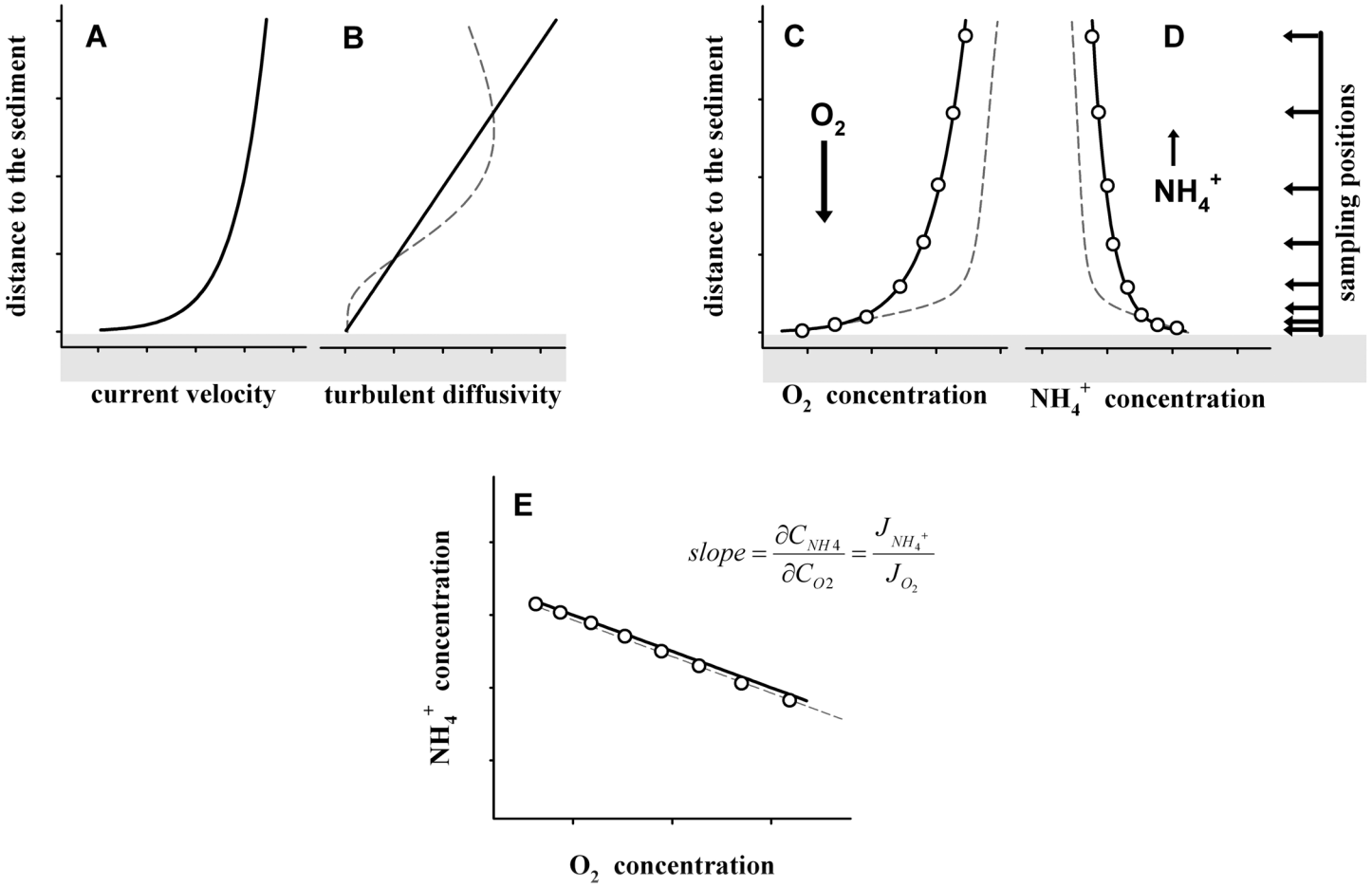

Fig. 1. Modeled profiles of current velocity (A), turbulent diffusivity (B), and oxygen and ammonium concentrations (C + D), assuming a steady state flux across the sediment–water interface (arrows in C + D show the direction). The slope of the linear regression of ammonium over oxygen concentrations (E) equals the ratio of ammonium efflux over oxygen uptake. The profiles were modeled using the analytical solutions for the log-law (Eqs. 2-4, black lines). The shape of the nonlinear diffusivity profile (gray dashed lines) is arbitrary and exemplifies the case of an unspecific flow field. In this case, the oxygen and ammonium concentrations are not calculated analytically but modeled using the finite element modeling program Comsol. The 1-dimensional model solves the diffusion equation $0=\partial(D_T\,\partial C/\partial z)/\partial z$. The conditions (steady state, boundary fluxes and concentrations) for the analytical and the numerical models were the same. The arbitrary diffusivity profile results in different concentration profiles but does not affect the flux ratio (E).

defines the direction of the solute flux. In Fig. 1 C + D, oxygen is consumed and ammonium is released from the sediment.

Assuming that turnover rates in the BBL are negligible, the solute flux across the BBL is independent of the distance z, and thus, is equal to the flux across the sediment surface. The flux can be calculated according to Eq. 1 from the product of the concentration gradient $\partial C/\partial z$ and the turbulent diffusivity D_T at a given depth. The flux (J) of two solutes such as O_2 and NH_4^+ can be compared by expressing the flux ratio:

$$\frac{J_{NH_4^+}}{J_{O_2}} = \frac{D_T\ \partial C_{NH_4^+}\ /\ \partial z}{D_T\ \partial C_{O_2}\ /\ \partial z} \qquad (5)$$

The turbulent diffusion coefficient is a function of the flow field, and therefore, D_T is the same for every solute. Eq. 5 can be simplified to

$$\frac{J_{NH_4^+}}{J_{O_2}} = \frac{\partial C_{NH4}}{\partial C_{O2}} \qquad (6)$$

The term $\partial C_{NH4}/\partial C_{O2}$ can be expressed graphically by plotting NH_4^+ over O_2 concentrations (Fig. 1E). If O_2 and NH_4^+ concentrations show a linear relationship, the slope of the linear regression is simply $\partial C_{NH4}/\partial C_{O2}$, which is equal to the flux ratio $J_{NH_4^+}\ /\ J_{O_2}$. A linear relationship between O_2 and NH_4^+ concentrations indicates that the flux ratio does not change across the BBL and reflects the flux ratio across the sediment surface. A nonlinear relationship between O_2 and NH_4^+ concentrations would be indicative for a changing flux ratio across the BBL. A changing flux ratio can be caused by significant turnover rates within the BBL or by the transient mixing of two or more bottom water layers of different origin that carry different O_2 and NH_4^+ concentrations. The negative slope indicates that O_2 and NH_4^+ are transported in opposite directions. In Fig. 1E, the

slope of the linear regression specifies how many moles of NH_4^+ are released from the sediment in exchange for one mole of O_2 that is taken up by the sediment.

To establish the flux ratio, no information about the turbulent diffusivity profile is needed. Assuming a different diffusivity profile (dashed profile in Fig. 1B) caused by, for example, a density stratification of the BBL, the steady state O_2, and NH_4^+ fluxes would result in different concentration gradients (dashed profiles in Fig. 1C + D), but they result in the same linear relationship between O_2 and NH_4^+ concentrations (dashed profile in Fig. 1E). Another case are transient flow regimes (for example from low to high current velocities), which cause transient diffusivities. Under these conditions, concentration gradients are re-adjusted causing transient fluxes within the BBL. However, the fluxes of the different solutes change proportionally and the flux ratio remains unaffected.

In addition to the example shown in Fig. 1, the flux ratio of nutrients over oxygen such as $J_{NO_3^-} / J_{O_2}$, $J_{NO_2^-} / J_{O_2}$, and $J_{PO_4^{3-}} / J_{O_2}$ can be derived from the respective concentration gradients. Subsequently, the relative efflux of fixed nitrogen (N_{fix}=NH_4^++NO_3^-+NO_2^-) and phosphate can be compared with the Redfield ratio and the C:N:P ratio of the surface sediment to establish an oxygen-nutrient flux balance between water column and sediment.

Sampling the BBL

Two different gears were applied to sample the BBL. In a first study, we used a Bottom Water Sampler (BWS) that was previously described by Sauter et al. (2005). The BWS consists of 6 horizontally aligned free flow bottles (volume: 6L) mounted to a central axis (240 cm high), which is fixed to a lead weighted bottom frame of 80 × 80 cm. The bottles can be vertically adjusted to different height levels. Free rotation of the instrument around the vertical axis allows the bottles to align with the bottom current. This is supported by a current vane attached to the axis. When the BWS is deployed to the seafloor a bottom switch starts the burn wire mechanism after a preselected time delay. We used a time delay of 15 min that allows the complete exchange of the bottle volume with bottom water and ensures that suspended sediment particles are flushed away. When the wire breaks, a mechanical releaser closes the lids of all bottles simultaneously. Subsequently, the BWS is retrieved and subsamples for nutrient and oxygen concentrations as well as for oxygen consumption measurements can be taken.

In a second study, we increased the vertical sampling resolution using a novel benthic boundary layer sampler named BBL profiler (Fig. 2, right image). The BBL profiler consists of a triangular frame that has a slider attached to one of the three legs. The slider is connected to a thread rod, which is driven by an electric motor. The slider moves vertically across the first meter above the sediment surface, stopping at programmed distances to measure for a time interval of 4 min. The slider carries an oxygen optode (Model 3830, response time < 25 s, Aanderaa), a sensor measuring conductivity, temperature, and depth (CTD) (YSI, 600XLM-M) and an acoustic doppler velocimeter (ADV) (Vectrino Nortek). Unfortunately, the ADV did not work properly, and we had to discard most of the measurements. A 12-channel peristaltic pump (KC, Denmark) is used to draw water samples for nutrient analysis from 0.07 to 1.8 m above the sediment surface. The inlets for the nutrient samples are fixed to a rod (2 m high) that is mounted next to

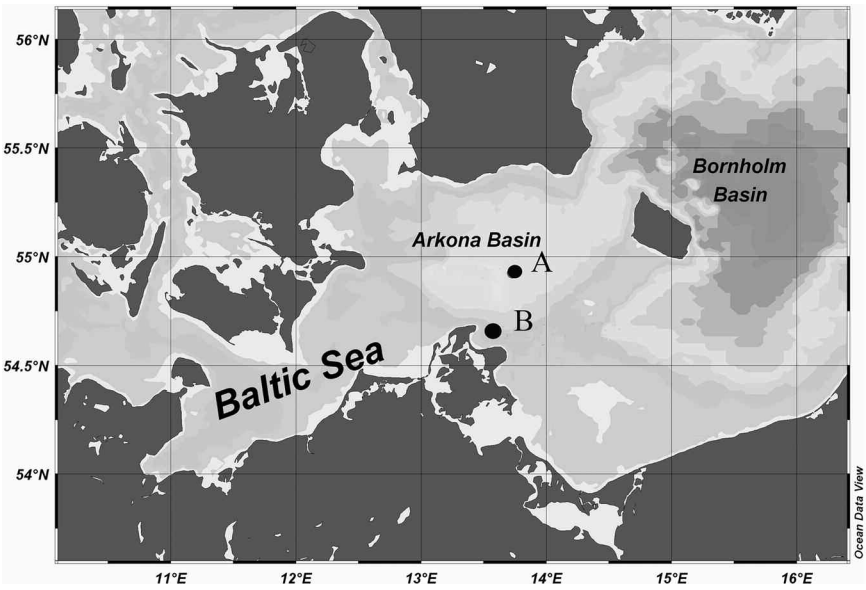

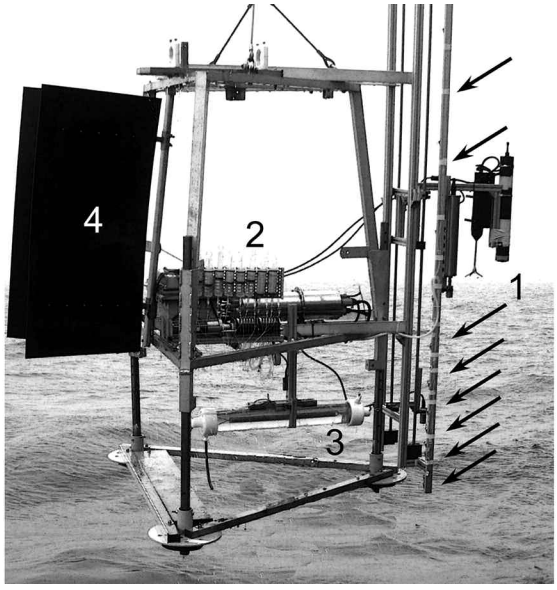

Fig. 2. (Left) The location of the sampling sites A and B in the Arkona Basin of the Baltic Sea. (Right) The BBL-Profiler, deployed during the second study at station B. The numbers mark: (1) The slider, carrying O_2-Optodes, ADV, and CTD; (2) Electronics, syringes and a 12-channel peristaltic pump; (3) The BWS free flow bottle; (4) A vane is attached to the frame to direct the Profiler toward the water current. The arrows mark inlets from where water samples were drawn.

the slider. From the inlets, water samples are drawn into Teflon tubing with a peristaltic pump and pressed into plastic syringes (100ml). The pump is programmed to run 10 minutes.

In addition to the nutrient sampling, a BWS free-flow bottle with a burn wire mechanism is mounted 35cm above the sediment surface to take samples for particle filtration and oxygen consumption measurements. All sensors, pumps, motors and burn wires are supplied by a 24 V battery and are operated by a programmable control unit. A vane attached to the frame allows directing the slider into the bottom current before it is lowered to the ground. The BBL-Profiler was deployed to the sea floor for about 2.5 hours while connected to a surface marker buoy. The sampling procedure started with a time delay of 30 minutes to allow the drift of sediment, which is artificially resuspended when the sampler is placed on the sediment.

The following section describes the BBL sampling and the subsequent chemical analysis of samples during two different studies. Nutrient and oxygen concentration gradients are processed as mentioned above. In addition, supplementary data such as particulate C:N ratios, oxygen uptake and denitrification rates from sediment incubation experiments are presented, which allow the calculation of a nitrogen flux balance and a comparison with the calculated flux ratios.

Assessment

Study site and supplementary sampling

For the first study, sediment and water samples were collected in September 2006 at station A (Fig. 2, left image), close to the center of the Arkona Basin, Baltic Sea (N 54° 46.50′, E 13° 49.00′, depth 42.4 m). For the second study, samples were collected in June 2007 at station B, at the periphery of the Arkona Basin (N 54° 39.18′, E 13° 28.21′, depth 20.0 m). At stations A and B, the BBL was sampled with the Bottom Water Sampler (BWS) and the BBL-Profiler, respectively. At station A, only 4 of 6 BWS bottles could be used for sampling. The water above the BWS was sampled using a Sea-Bird CTD (SBE 19-04) and regular Niskin bottles. Subsamples were taken for oxygen and nutrient analysis as well as for particle filtration and oxygen consumption measurements.

Sediment was sampled only at station A by using a multicorer equipped with acrylic liners of 10 cm diameter. Subsamples of ∅ 3.6 cm cores were taken for oxygen uptake and denitrification experiments. Results of these experiments were compared to the denitrification and oxygen uptake rates derived from BBL concentration gradients. Porewater from a ∅ 10 cm core was sampled on board by inserting Rhizon Soil Solution Samplers (Seeberg-Elverfeldt et al. 2005) with a vertical resolution of 1 cm (between 0 and 5 cm depth) and 2 cm (between 5 and 22 cm depth).

Chemical analysis

At station A, oxygen and ammonium concentrations in the water column were measured immediately on board by Winkler titration and fluorimetric analysis (Holmes et al. 1999), respectively. At station B, oxygen concentrations were measured in situ by an oxygen optode attached to the slider of the BBL-Profiler. Water column samples for nutrient analysis (i.e., NH_4^+, NO_3^-, NO_2^-, and PO_4^{3-}) were stored in centrifuge tubes at –20°C until measured in the laboratory (autoanalyzer, TRAACS 800, Bran & Luebbe). Porewater samples (only station A) for NO_3^- and NO_2^- measurements were stored frozen in Eppendorf vials (2 mL) until measured with a chemoluminescence NOx analyzer (Thermo Environmental Instruments) according to Braman and Hendrix (1989). Porewater samples (2 mL) for NH_4^+ measurements were amended with 0.1 mL saturated $HgCl_2$, stored without headspace at 4°C and measured by flow injection according to Hall and Aller (1992).

Oxygen consumption

Oxygen uptake of the sediment from station A was determined on board in two sediment cores (∅ 3.6 cm) by measuring the oxygen decrease in the overlying water over time. During the incubation, the overlying water was mixed by small magnetic stirrers placed inside the cores and driven by a large external magnet. The cores were sealed with rubber stoppers, leaving no gas phase inside. Oxygen concentration was measured with needle optodes (PreSens, Precision Sensing GmbH, Germany) that were pushed through the rubber stoppers. Measurements were performed in the dark at in situ temperatures (15°C).

Denitrification

Sedimentary denitrification rates (only station A) were determined using the isotope pairing technique (IPT) described in detail by Nielsen (1992). Experiments were carried out on board. In 15 sediment cores (∅ 3.6 cm) the overlying water column (~127 mL) was amended with $^{15}NO_3^-$ to a final concentration of 50 µmol L^{-1}. After preincubation of the open cores for 12 h, dinitrogen gas was trapped by sealing all cores with rubber stoppers and incubating without a gas phase. At each time point (0, 1, 2, 5, and 9 h), 3 cores were sampled by mixing the top 3 cm of the sediment with the overlying water, transferring a slurry sample into 12 mL gas tight vials (Exetainers, Labco) and fixing the sample with 100 µL saturated $HgCl_2$ solution. The incubation was performed in the dark at in situ temperatures. In the laboratory, a 2 mL helium headspace was introduced into the vial. After equilibration, the N_2 isotope ratio ($^{28}N_2$, $^{29}N_2$, and $^{30}N_2$) of the headspace was determined by gas chromatography-isotopic ratio mass spectrometry by direct injections from the headspace according to Kuypers et al. (2005). Concentrations of $^{30}N_2$ and $^{29}N_2$ were normalized to $^{28}N_2$ and calculated as excess relative to air. N_2 production rates were calculated from the slope of $^{29}N_2$ and $^{30}N_2$ increase over time and denitrification of $^{15}NO_3^-$ (D_{15}) and $^{14}NO_3^-$ (D_{14}) was calculated after Nielsen (1992) from the production of $^{30}N_2$ and $^{29}N_2$ according to $D_{15}={}^{29}N_2+2\ {}^{30}N_2$ and $D_{14}=D_{15}({}^{29}N_2/2\ {}^{30}N_2)$.

Results

At station A, the water column was stratified due to a salinity gradient—a permanent feature in the Arkona Basin

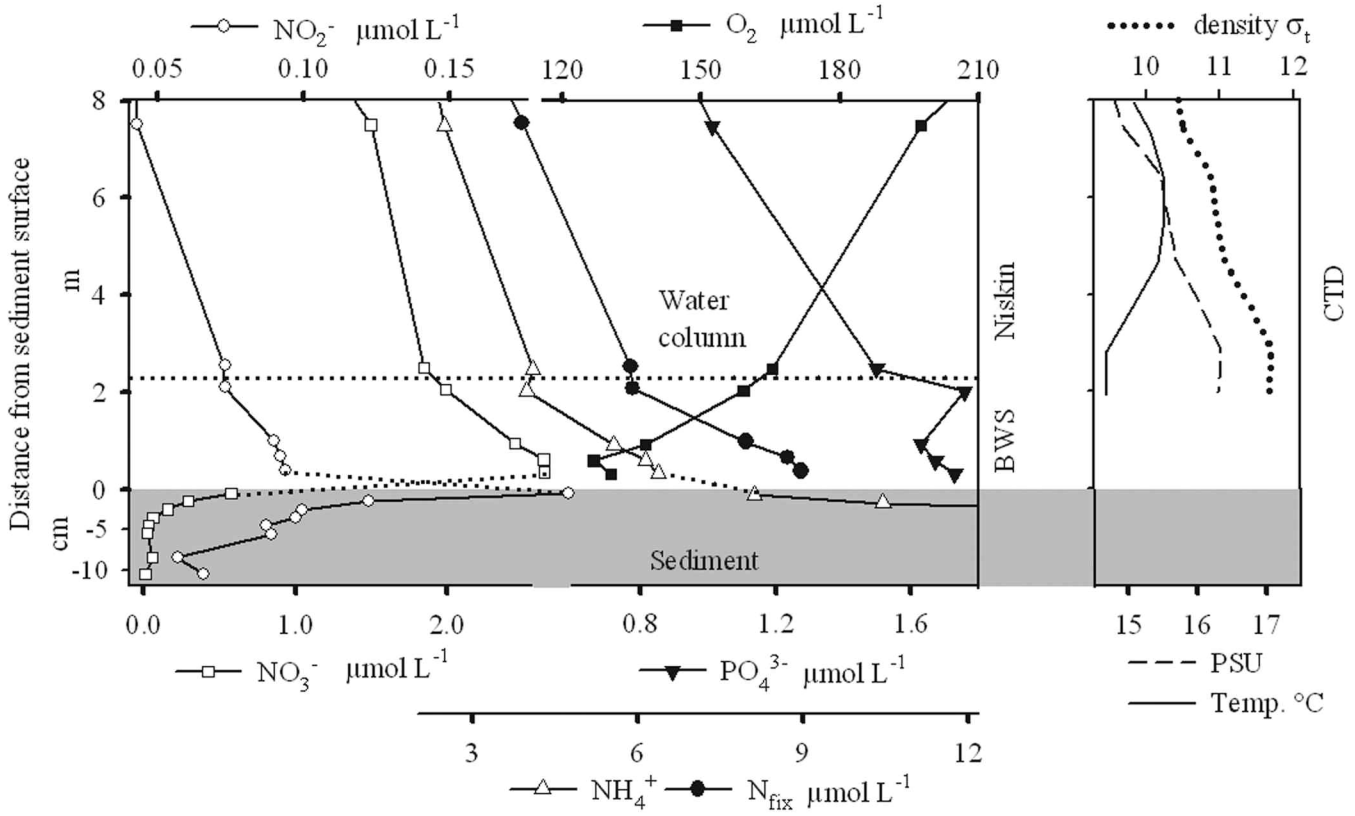

Fig. 3. Station A. Left side: Nutrient and oxygen concentrations across the BBL and in the porewater. The gray area marks the sediment and the dotted horizontal line separates the sampling range of the BWS from the sampling range of the Niskin bottles. N_{fix} was calculated as the sum of NH_4^+, NO_2^-, and NO_3^-. Concentration profiles in sediment and BBL are connected by straight dotted lines. Right side: Salinity, temperature, and density measured with the CTD.

(Gustafsson 2001). The salinity gradient was present down to 3 m above sediment (Fig. 3). In the BBL, the concentrations of all nitrogen species, i.e., NH_4^+, NO_2^-, and NO_3^-, and the concentration of PO_4^{3-} increased toward the sediment whereas oxygen concentration decreased. All gradients, with the exception of phosphate, increased in the lowermost 2 m of the water column. The atomic C/N ratio of the particles at 0.35 m and 0.6 m above the sediment was 10.1 and 10.3, respectively. Concentrations of porewater NO_2^- and NO_3^- decreased exponentially with depth while NH_4^+ concentrations increased linearly (total profile not shown in Fig. 3). The combined BBL and porewater profiles suggests that NH_4^+ was released due to mineralization processes deeper in the sediment from where it diffused toward the sediment surface and into the water column. The maximum concentrations of NO_2^- and NO_3^- at the sediment surface indicate that NH_4^+ was oxidized at the sediment surface (i.e., nitrification). In turn, NO_2^- and NO_3^- were transported from the sediment surface into the water column as well as deeper into the sediment where they were converted to N_2 gas via denitrification. Ongoing denitrification in the sediment as determined by the IPT method was confirmed by the linear increase of $^{29}N_2$ and $^{30}N_2$ concentrations over time (R^2 = 0.90, and R^2 = 0.82, respectively). The calculated loss of $^{14}NO_3^-$ due to

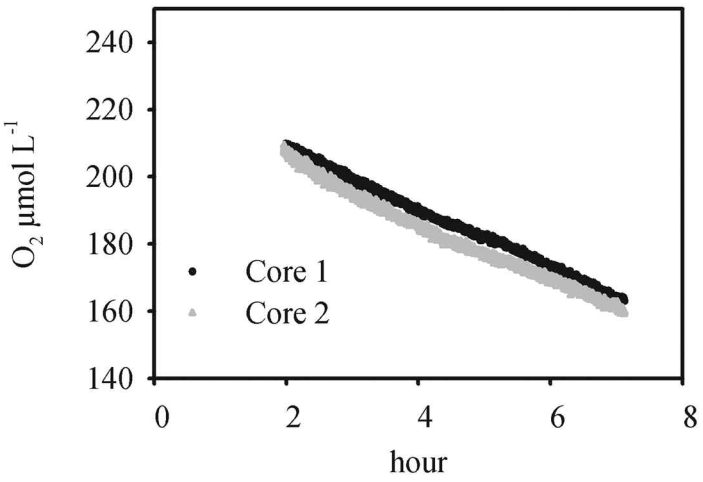

Fig. 4. Station A. Decrease of oxygen concentrations in the overlying water of two sediment cores. The calculated oxygen fluxes into the sediment were 10.5 and 10.4 mmol m^{-2} d^{-1} (R^2 = 0.989 and R^2 = 0.996, respectively).

denitrification was 0.33 mmol N m^{-2} d^{-1}. Oxygen uptake of the sediment as determined from the two core incubation experiments was 10.5 and 10.4 mmol m^{-2} d^{-1}, respectively (Fig. 4).

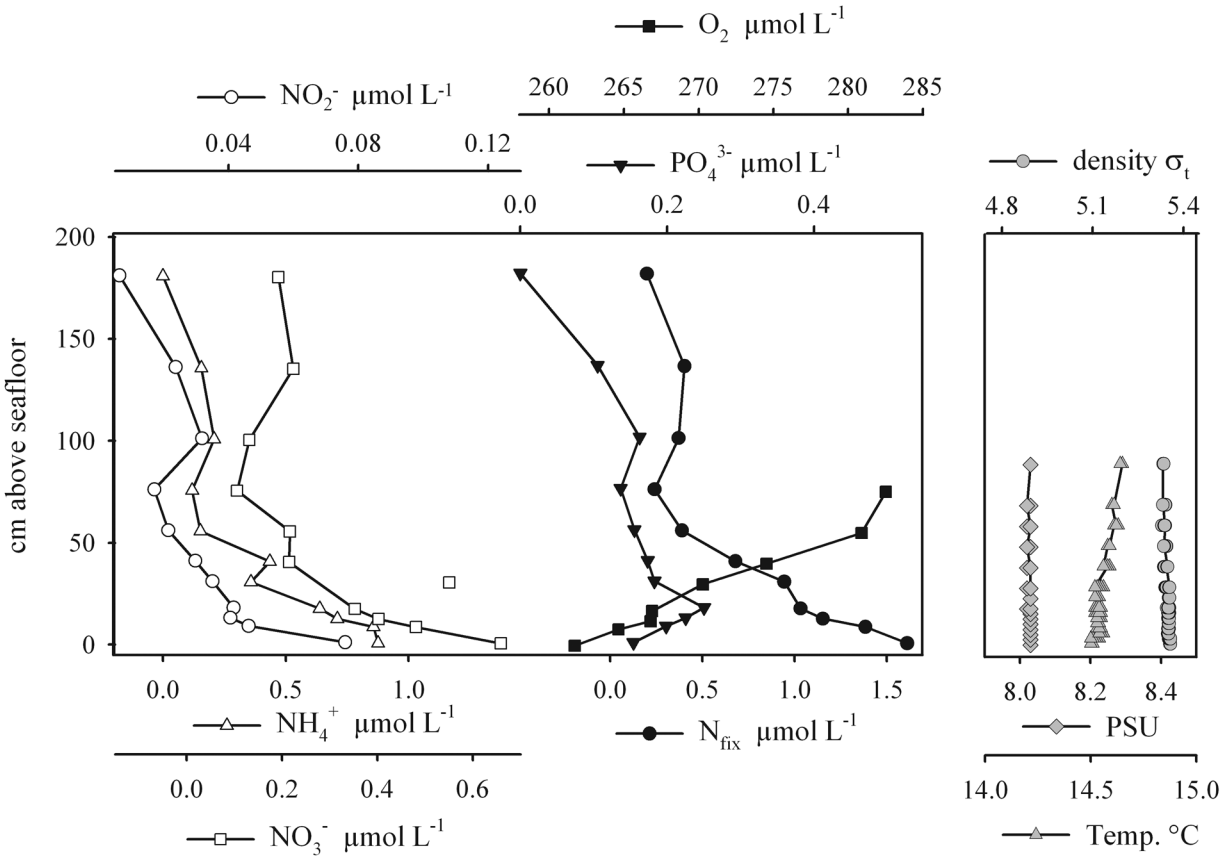

Fig. 5. Station B. Left side: Nutrient and oxygen concentrations across the BBL. The NO_3^- concentration at 30 cm above the sediment was discarded as outlier and not used for further calculations. Right side: salinity, temperature, and density across the BBL.

The organic carbon content of the surface sediment was 3.3 wt% and the atomic C/N ratio was 10.0 ± 0.3. Similar C/N ratios of bottom water particles and sediments in the central Arkona Basin were reported by Emeis et al. (2002).

At station B, no density stratification due to salinity or temperature gradients was observed (Fig. 5). Highest concentrations of NH_4^+, NO_2^-, and NO_3^-, and lowest concentrations of O_2 were found close to the sediment surface. PO_4^{3-} concentrations did not show a clear trend, which we attribute to the fact that PO_4^{3-} concentrations were at the detection limit. The particle concentration at 35 cm above the sediment was 4 mg/L. The atomic C/N ratio of the particles was 7.1.

Calculation of flux ratios

Following the procedure described in the method section, nutrient concentrations of each station were plotted versus the corresponding oxygen concentrations (Fig. 6). A significant linear relationship was found for all nutrients ($P < 0.05$ for PO_4^{3-} at station A, all others at least $P < 0.01$) except for PO_4^{3-} at station B, which was not used for further calculations. According to Eq. 6, flux ratios were derived from the slope of the linear regression. All slopes in Fig. 6 have a negative sign indicating that nutrients and oxygen were transported in opposite directions. In addition, the concentration of fixed nitrogen, defined as $N_{fix}=NH_4^+ + NO_3^- + NO_2^-$ was calculated for each sampling depth and plotted versus O_2 to calculate the $J_{N_{fix}} / J_{O_2}$ flux ratio. The magnitude of all flux ratios are summarized in Table 1. At both stations, NH_4^+ was the major constituent of the nutrient efflux accounting for 75% (station A) and 62% (station B) of the total nitrogen flux ($J_{N_{fix}}$), whereas the contribution of the NO_3^- flux was 23% (station A) and 34% (station B). The ratio of the total nitrogen flux ($J_{N_{fix}}$) over the phosphate flux ($J_{PO_4^{3-}}$) was 8.3:1 (station A), which was significantly below the Redfield ratio of 16:1, suggesting the removal of fixed nitrogen from the sediments due to denitrification.

Calculation of the nitrogen balance

Applying the flux ratios, we balanced the oxygen and nutrient exchange across the sediment–water interface with the organic matter mineralization in the sediment. The fluxes and processes involved are presented as a schematic drawing in Fig. 7 and will be explained in the following. In sediments underlying well-oxygenated bottom waters, oxygen is the ultimate electron acceptor of almost all electron equivalents released during the oxidation of organic matter (Canfield et al. 2005; Thamdrup and Canfield 2000). Thus, the oxygen uptake of the sediment can be used as a proxy for the total carbon mineralization:

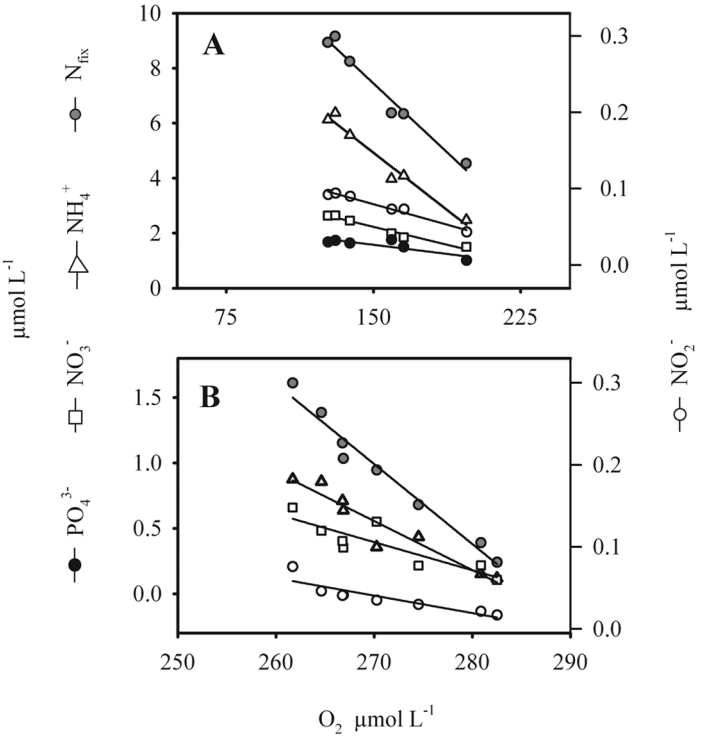

Fig. 6. Concentrations of nitrite, nitrate, ammonium, total fixed nitrogen, and phosphate (only station A) plotted over oxygen concentrations at station A and station B.

C mineralization = O_2 respiration + inorganic reoxidation = O_2 consumption

However, part of the oxygen that is taken up by the sediment is used to oxidize an unknown amount of NH_4^+ to NO_2^- and further to NO_3^- (nitrification). In turn, some of the NO_2^- and NO_3^- diffuses upward into the water column ($J_{NO_2^-}$, $J_{NO_3^-}$), whereas a fraction of the NO_3^- diffuses downward where it is reduced to N_2 via denitrification. The complete nitrification reaction can be expressed as two separate processes:

$$NH_4^+ + 1.5O_2 \rightarrow NO_2^- + H_2O + 2H^+ \quad (7)$$

$$NO_2^- + 0.5O_2 \rightarrow NO_3^- \quad (8)$$

The oxidation of organic carbon to CO_2 via denitrification requires 0.8 NO_3^- (Canfield et al. 1993):

$$C_{org} + 0.8\,NO_{3Den}^- \rightarrow CO_2 + 0.4\,N_2 \quad (9)$$

Here and in the following, all nitrate reduced to N_2 via denitrification is denoted as NO_{3Den}^-.

In summary, the total carbon mineralization is the sum of the oxygen uptake, corrected by the oxygen used for nitrification, and the carbon mineralized via denitrification:

Table 1. Nutrient fluxes relative to oxygen flux derived from the slope of the linear regression between the oxygen and the respective nutrient concentrations in the BBL. R^2 gives the coefficient of determination.

(Fluxes relative to J_{O_2})		J_{O_2}	$J_{PO_4^{3-}}$	$J_{N_{fix}}$	$J_{NH_4^+}$	$J_{NO_3^-}$	$J_{NO_2^-}$
Station A	flux %	100	0.89	7.4	5.6	1.7	0.07
	R^2	1	0.722	0.972	0.968	0.969	0.975
Station B	flux %	100	(0.28)	6.1	3.8	2.1	0.21
	R^2	1	(0.302)	0.970	0.917	0.856	0.793

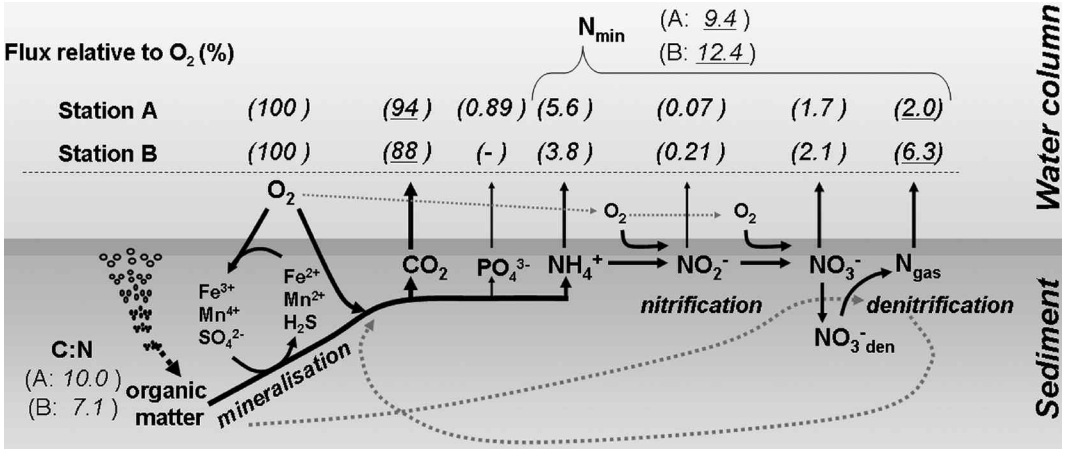

Fig. 7. Schematic diagram of nutrient/oxygen fluxes and organic matter mineralization in and above the sediment. The flux values for station A and B are taken from Table 1. Underlined values denote fluxes calculated according to Eqs. 10, 11, and 12. N_{min} denotes the total mineralized nitrogen. All fluxes are expressed as percentage of the O_2 flux.

$$C_{min} = J_{O_2} - \left(2\,J_{NO_3^-} + 1.5\,J_{NO_2^-} + 2\,J_{Den\,NO_3^-}\right) + 0.8\,J_{Den\,NO_3^-} \quad (10)$$

whereas the total nitrogen mineralization is the sum of the efflux of NH_4^+, NO_2^-, and NO_3^- into the water column and the NO_3^- used for denitrification:

$$N_{min} = J_{NH_4^+} + J_{NO_2^-} + J_{NO_3^-} + J_{Den\,NO_3^-} \quad (11)$$

As first approximation we assume that the C:N ratio of the mineralized organic matter in the sediment reflects the C:N ratio of the particulate organic matter, which now can be expressed as:

$$C:N = \frac{J_{O_2} - \left(2\,J_{NO_3^-} + 1.5\,J_{NO_2^-} + 2\,J_{Den\,NO_3^-}\right) + 0.8\,J_{Den\,NO_3^-}}{J_{NH_4^+} + J_{NO_2^-} + J_{NO_3^-} + J_{Den\,NO_3^-}} \quad (12)$$

By substituting the measured C:N ratio of the surface sediments and the flux ratios from Table 1, $J_{Den\,NO_3^-}$ remains as the only unknown variable. Solving Eq. 12 for $J_{Den\,NO_3^-}$ leads to:

$$J_{Den\,NO_3^-} = \frac{J_{O_2} - 1.5\,J_{NO_2^-} - 2\,J_{NO_3^-} - C:N\left(J_{NH_4^+} + J_{NO_2^-} + J_{NO_3^-}\right)}{C:N + 1.2} \quad (13)$$

Applying Eqs. 10, 11, and 13, the fluxes of mineralized carbon, mineralized nitrogen, and nitrogen gas (i.e., $J_{Den\,NO_3^-}$) were calculated (Fig. 7). The flux of mineralized nitrogen can be divided into nitrification ($J_{Nit} = J_{NO_3^-} + J_{Den\,NO_3^-}$), denitrification ($J_{Den\,NO_3^-}$), and the efflux of fixed nitrogen ($J_{N_{flx}} = J_{NH_4^+} + J_{NO_2^-} + J_{NO_3^-}$) (*see* Table 2). Of the total mineralized nitrogen 78% (station A) and 49% (station B) were released to the water column, whereas 22% (station A) and 51% (station B) were lost due to denitrification. Of the total mineralized nitrogen 40% (station A) and 68% (station B) was oxidized to nitrate, with nitrification accounting for 8% (station A) and 18% (station B) of the total oxygen demand of the sediment.

The relative contribution of heterotrophic denitrification to the total carbon oxidation varied from 1.7% at station A to 5.7% at station B. This agrees well with reported values of 1-8% in the Kattegat (Rysgaard et al. 2001), 2% in Aarhus Bay (Jørgensen 1996), and 3-6% in the Skagerrak (Canfield et al. 1993). The flux ratio of calculated CO_2 over PO_4^{3-} (only station A) is 106, which represents exactly the Refield ratio. Finally, the calculated ratio of denitrification over oxygen uptake ($J_{Den\,NO_3^-}$ *in %* J_{O_2}) is 2% at station A. This compares well with the results from the core incubation experiments at station A, where denitrification was 0.33 mmol N m^- d^{-1} and oxygen uptake was 10.5 mmol O_2 m^- d^{-1}, which results in a ratio of denitrification over oxygen uptake of 3.1%.

Discussion

Concentration gradient measurements

The aim of this study was to present novel instrumentation and sampling strategies for the measurement of nutrient and oxygen concentration gradients in the BBL, and to provide the theoretical basis for a meaningful interpretation of these gradients. As expected from theoretical considerations (*see* Fig. 1), concentration gradients increased toward the sediment. The vertical sampling resolution, especially in the first 50 cm above the sediment, was significantly improved with the new BBL-Profiler. With this instrument, steep concentration gradients were resolved close to the sediment surface (Fig. 5). The concentration gradients as such provide valuable information. At both stations, minimum O_2 and maximum nutrient concentrations at the sediment surface indicated that the sediment was a net O_2 sink and a net source of PO_4^{3-}, NH_4^+, NO_2^-, and NO_3^-. Hence, there was no NO_2^- and NO_3^- flux from the overlying water into the sediment, which in turn, implies that denitrification, as the main NO_2^- and NO_3^- reducing processes in the sediment, was fully coupled to nitrification at the sediment surface.

The flux ratio approach

Plots of nutrients versus oxygen concentrations in the BBL revealed linear relationships (Fig. 6). According to Eq. 6, the slopes of the linear correlations can be interpreted as the ratio of the specific nutrient flux over the oxygen flux. The linearity of these correlations also indicates that the flux ratios do not change across the BBL, and thus, reflect the flux ratios across the sediment surface. This interpretation is supported by the results from the nutrient-oxygen flux balance (Fig. 7, Table 2) that agree well with the C:P Redfield ratio and the experimental oxygen/denitrification flux measurements.

In general, we assumed that the flux across the BBL equals the flux across the sediment–water interface. However, this assumption can be violated by either high mineralization rates within the BBL or by the transient mixing of distinct water layers in the BBL that carry different solute concentrations (i.e., end-member mixing). As a result the solute flux caused by sediment activity would be overprinted by the fluxes due to end-member mixing and BBL mineralization. In the BBL, the latter fluxes are a function of the vertical dimension (z), whereas the flux due to sediment activity is not. Therefore, all flux ratios that are influenced by end-member mixing and BBL mineralization would result in a non-linear relationship between the respective solute concentrations. The linear relationship that we found in this study suggests that the fluxes caused by sediment activity were dominant. This is supported by the low oxygen uptake rates (<2 µM d^{-1}, station A and <5 µM d^{-1}, station B) determined experimentally for BBL water samples (data not shown here).

The flux ratio approach presented here is applicable without knowledge of the turbulent diffusivity profile. The approach is, therefore, unaffected by transient current velocities and diffusivities (see gray dashed profiles in Fig. 1). This is of significant advantage because the current velocity profile in BBLs with slow, alternating currents is often not in steady state and, therefore, cannot be described by the log-law (Lorke et al. 2002). The main assumption for most flux measurements (e.g., from porewater profiles, chamber incubations, or eddy correlation measurements) is that benthic turnover rates of oxygen and nutrients are considered constant during the mea-

Table 2. From left to right: The efflux of fixed nitrogen, denitrification, and nitrification relative to the total mineralized nitrogen, the contribution of denitrification to the total carbon mineralization, the C:P ratio, and the denitrification relative to the oxygen uptake.

(% of N_{min})	J_{Nfix}	$J_{Den\ NO_3^-}$	J_{Nit}	$J_{Den\ CO_2}$ (% $J_{tot\ CO_2}$)	J_{CO_2} / $J_{PO_4^{3-}}$		$J_{Den\ NO_3^-}$ (% J_{O_2})	
					flux ratio	Redfield	flux ratio	core incubation
Station A	78	22	40	1.7	106	106	2.0	3.1
Station B	49	51	68	5.7	—	—	6.3	—

Table 3. Left column: Absolute fluxes of oxygen and nutrients at station A. Right column: total mineralized nitrogen and rates of nitrification and denitrification at station A.

mmol m^{-2} d^{-1}	J_{O_2}	$J_{PO_4^{3-}}$	J_{Nfix}	$J_{NH_4^+}$	$J_{NO_3^-}$	$J_{NO_2^-}$	$J_{N\ tot}$	$J_{Den\ NO_3^-}$	J_{Nit}
Station A	10.45	0.093	0.77	0.58	0.18	0.008	0.98	0.21	0.39

surement. However, because the turbulent regime in the bottom water affects the solute transport in the turbulent boundary layer (Holtappels and Lorke 2010) as well as in the diffusive boundary layer (Lorke et al. 2003), a transient turbulent flow can result in variable solute concentrations at the sediment surface and, in the case of oxygen, in variable oxygen penetration depths and oxygen uptake rates (Glud et al. 2007). Nevertheless, it is reasonable to assume that the short-term variability of oxygen uptake and nutrient release is nearly proportional, thus minimizing the variability of their flux ratio.

A major advantage of the flux ratio approach is that small-scale horizontal heterogeneities of the solute flux are averaged during the turbulent vertical mixing. Because measurements are taken above the sediment surface they integrate over a large surface area that contributes to the flux and account for spatial variability in bioirrigation, sediment structure, and macrofauna distribution. The new approach is noninvasive and can also be used to determine benthic fluxes from sandy sediments and shell beds, which are extremely difficult to obtain with benthic chamber and sediment coring techniques. However, large-scale heterogeneities in the nearby upstream direction such as those found at transitions from plain sediment to sea grass need to be considered. An estimate of the surface area that contributes to the flux—the so called footprint—can be obtained using the method described by Berg et al. (2007). In principle, the sampled area should not contain large-scale heterogeneities in the footprint defined by the uppermost sampling elevation, whereas small-scale heterogeneities should be small enough to be averaged within the footprint of the lowermost sampling elevation. For the sampling sites in this study, we assumed negligible effects of large-scale heterogeneities.

From relative to absolute fluxes

In this study, nutrient fluxes were expressed as fluxes relative to oxygen. These flux ratios provided valuable information to establish a nitrogen balance and to estimate the proportional N-loss from the sediment (Fig. 7). In the following, we briefly discuss how concentration gradients and flux ratios can be converted into absolute flux estimates. In general, a single measurement of an absolute nutrient or oxygen flux is sufficient to determine the absolute fluxes of all other solutes from their flux ratio. As an example, we use the oxygen flux estimated from the core incubations at station A (10.45 mmol m^{-2} d^{-1}) and the previously determined flux ratios (Table 1) to calculate the absolute flux for every nutrient (Table 3). Also fluxes such as for nitrite and phosphate can be quantified. Most promising is the combination of the flux ratio approach with the eddy correlation technique for oxygen fluxes (Berg et al. 2003; Brand et al. 2008; McGinnis et al. 2008). Eddy correlation flux measurements are performed in the BBL, and therefore, feature most of the advantages mentioned above for the flux ratio approach. Since the eddy correlation technique measures the instantaneous flux of a solute in the turbulent flow field, it is based on extremely fast and accurate concentration measurements as performed only by electrochemical microsensors for oxygen and eventually for sulfide and calcium. The combination of the eddy correlation technique with the flux ratio approach described here would considerably extend the number of solutes for which the absolute flux can be measured in a non-invasive way.

A promising modification of the flux ratio approach is the correlation of solute concentration gradients $\partial C / \partial z$ with gradients of average current velocities $\partial \bar{U} / \partial z$. In analogy to the solute flux, the momentum flux in turbulent shear flow is assumed to be proportional to the mean velocity gradient (Tennekes and Lumley 1972):

$$\langle u\, w \rangle = -\nu_T \frac{\partial \bar{U}}{\partial z} \tag{14}$$

where the constant of proportionality (ν_T) is denoted as turbulent viscosity and the momentum flux is expressed as $\langle uw \rangle$, i.e., time averaged covariance of turbulent velocities in the mean flow direction (u) and vertical direction (w). Fluid density is omitted on both sides of Eq. 14. Combining Eqs. 1 and 14, the ratio of solute flux to momentum flux is:

$$\frac{J}{\langle u\, v \rangle} = \frac{D_T\, \partial C / \partial z}{\nu_T\, \partial \bar{U} / \partial z} \tag{15}$$

Assuming that the ratio ν_T/D_T is close to one, Eq. 15 is simplified to:

$$\frac{J}{\langle u\, v\rangle} = \frac{\partial C}{\partial \bar{U}} \quad (16)$$

Tennekes and Lumley (1972) described a similar relation known as 'Reynolds' analogy, which relates heat flux and momentum flux. Equation 16 can be used to estimate the solute flux if concentration and velocity gradients and the momentum flux is known. Although the velocity measurements during this study were problematic, measurements of average velocity profiles and turbulent velocities (e.g., u and w) are usually reliable and easy to perform using acoustic Doppler current profilers (ADCP) and ADVs, respectively. However, the covariance measurement $\langle uw\rangle$ is very sensitive to the vertical alignment of the ADV and correction calculations are not trivial (Wilczak et al. 2001).

Finally, the concentration gradients can be combined with estimates of D_T to calculate the flux. The log-law predicts a linear increase of D_T (equation 3). If one assumes that the log-law was applicable under the measurement conditions, it should be possible to use reasonable estimates of u_* and fit Eq. 4 to the measured concentration gradients to determine the flux J. However, from the measured gradients we derived unrealistically high fluxes of e.g., $J_{NH_4^+} > 10$ mmol m^{-2} s^{-1} at station B, even for very small $u_* < 1.5$ mm s^{-1}. The corresponding D_T was ~1×10^{-4} m^2 s^{-1} at 15 cm above the sediment (calculated from Eq. 3). In contrast, D_T calculated from measured oxygen concentration gradients and assumed oxygen fluxes of ~10 mmol m^{-2} d^{-1} range between 10^{-6} to 10^{-5} m^2 s^{-1}. Obviously, the log-law overestimates D_T under the present conditions of low current velocity and cannot be applied here. This agrees well with the results of Holtappels and Lorke (2010) who compared several approaches to determine D_T under variable conditions in the BBL and found that the log-law overestimated D_T up to 2 orders of magnitude.

In summary, there are several possibilities to obtain absolute fluxes by combining (i) flux ratios with eddy correlation measurements, (ii) concentration gradients with momentum flux and velocity gradients, and (iii) concentration gradients with turbulent diffusivities. However, the application of these additional measurements requires detailed insights into the state of the boundary flow.

Comments and recommendations

The detection of concentration gradients is a prerequisite for the flux ratio approach presented here. The magnitude of the concentration gradients depends on both, the turbulent diffusivity and the respective solute flux. For a moderate flux, high current velocities lead to high turbulent mixing which results in eventually undetectable concentration gradients. This clearly limits the applicability of the flux ratio approach to low current velocities and low turbulent diffusivities. The diffusivities at station A and B ranged from 10^{-6} to 10^{-5} m^2 s^{-1} when calculated from the oxygen concentration gradients and the oxygen flux of 10 mmol m^{-2} d^{-1} (measured at station A). These diffusivities compare well with those reported by Lorke (2007) and Lorke et al. (2008) for the BBL of a large lake. In the Baltic Sea, the absence of tides leads to low average current velocities in the range of a few cm s^{-1} (Christiansen et al. 2002) that are comparable to those found in lakes. The flux ratio approach, therefore, seems to be limited to low energy flow as found in lakes, enclosed seas, and low-energy shelf systems. However, the method can be improved by increasing the vertical sampling resolution and by measuring even closer to the sediment surface where turbulent diffusion is reduced.

References

Berg, P., and others. 2003. Oxygen uptake by aquatic sediments measured with a novel non-invasive eddy-correlation technique. Mar. Ecol. Progr. Ser. 261:75-83 [doi:10.3354/meps261075].

———, H. Roy, and P. L. Wiberg. 2007. Eddy correlation flux measurements: The sediment surface area that contributes to the flux. Limnol. Oceanogr. 52:1672-1684.

Berner, R. A. 1982. Burial of organic-carbon and pyrite sulfur in the modern ocean—its geochemical and environmental significance. Am. J. Sci. 282:451-473 [doi:10.2475/ajs.282.4.451].

Braman, R. S., and S. A. Hendrix. 1989. Nanogram nitrite and nitrate determination in environmental and biological-materials by vanadium(III) reduction with chemi-luminescence detection. Anal. Chem. 61:2715-2718 [doi:10.1021/ac00199a007].

Brand, A., D. F. McGinnis, B. Wehrli, and A. Wüest. 2008. Intermittent oxygen flux from the interior into the bottom boundary of lakes as observed by eddy correlation Limnol. Oceanogr. 53:1997-2006 [doi:10.4319/lo.2008.53.5.1997].

Canfield, D., B. Thamdrup, and E. Kristensen [eds.]. 2005. Aquatic geomicrobiology. Elsevier.

Canfield, D. E., and others. 1993. Pathways of organic-carbon oxidation in 3 continental-margin sediments. Mar. Geol. 113:27-40 [doi:10.1016/0025-3227(93)90147-N].

Christiansen, C., and others. 2002. Material transport from the nearshore to the basinal environment in the southern Baltic Sea-I. Processes and mass estimates. J. Mar. Syst. 35:133-150 [doi:10.1016/S0924-7963(02)00126-4].

Dade, B. D., A. Hogg, and B. P. Boudreau. 2001. Physics of flow above the sediment-water interface, p. 4-43. *In* B. P. Boudreau and B. B. Jørgensen [eds.], The benthic boundary layer: transport processes and biogeochemistry. Oxford Univ. Press.

Emeis, K., and others. 2002. Material transport from the near shore to the basinal environment in the southern Baltic Sea-II: Synthesis of data on origin and properties of material. J. Mar. Syst. 35:151-168 [doi:10.1016/S0924-7963(02)00127-6].

Glud, R. N., J. K. Gundersen, B. B. Jørgensen, N. P. Revsbech,

and H. D. Schulz. 1994. Diffusive and total oxygen-uptake of deep-sea sediments in the eastern south-atlantic ocean - in-situ and laboratory measurements. Deep-Sea Res. I 41:1767-1788 [doi:10.1016/0967-0637(94)90072-8].

———, J. K. Gundersen, N. P. Revsbech, B. B. Jørgensen, and M. Huttel. 1995. Calibration and performance of the stirred flux chamber from the benthic lander Elinor. Deep-Sea Res. I 42:1029-1042 [doi:10.1016/0967-0637(95)00023-Y].

———, P. Berg, H. Fossing, and B. B. Jørgensen. 2007. Effect of the diffusive boundary layer on benthic mineralization and O_2 distribution: A theoretical model analysis. Limnol. Oceanogr. 52:547-557 [doi:10.4319/lo.2007.52.2.0547].

Graf, G. 1992. Benthic-pelagic coupling—a benthic view. Oceanogr. Mar. Biol. 30:149-190.

———, and others. 1995. Benthic-pelagic coupling in the Greenland Norwegian Sea and its effect on the geological record. Geologische Rundschau 84:49-58 [doi:10.1007/BF00192241].

Gustafsson, B. G. 2001. Quantification of water, salt, oxygen and nutrient exchange of the Baltic Sea from observations in the Arkona Basin. Cont. Shelf Res. 21:1485-1500 [doi:10.1016/S0278-4343(01)00014-0].

Hall, P. O., and R. C. Aller. 1992. Rapid, small-volume, flow injection analysis for _CO2 and NH_4^+ in marine and freshwaters. Limnol. Oceanogr. 37:1113-1119 [doi:10.4319/lo.1992.37.5.1113].

Holmes, R. M., A. Aminot, R. Kerouel, B. A. Hooker, and B. J. Peterson. 1999. A simple and precise method for measuring ammonium in marine and freshwater ecosystems. Can. J. Fish. Aquat. Sci. 56:1801-1808 [doi:10.1139/cjfas-56-10-1801].

Holtappels, M., and A. Lorke. 2010. Estimating turbulent diffusion in a benthic boundary layer. Limnol. Oceanogr. Methods 9:29-41 [doi:10:4319/lom.2011.9.29].

Jørgensen, B. B. 1996. Case study—Aarhus Bay, p. 137-154. *In* B. B. Jørgensen and K. Richardson [eds.], Eutrophication in coastal marine ecosystems. American Geophysical Union.

———, and N. P. Revsbech. 1985. Diffusive boundary layers and the oxygen uptake of sediments and detritus. Limnol. Oceanogr. 30:111-122 [doi:10.4319/lo.1985.30.1.0111].

Kawanisi, K., and S. Yokosi. 1997. Characteristics of suspended sediment and turbulence in a tidal boundary layer. Cont. Shelf Res. 17:859-875 [doi:10.1016/S0278-4343(96)00066-0].

Kuypers, M. M. M., and others. 2005. Massive nitrogen loss from the Benguela upwelling system through anaerobic ammonium oxidation. Proc. Nat. Acad. Sci. U.S.A. 102:6478-6483 [doi:10.1073/pnas.0502088102].

Lorke, A. 2007. Boundary mixing in the thermocline of a large lake. J. Geophys. Res. Oceans 112, C09019, 10 PP [doi:10.1029/2006JC004008].

———, L. Umlauf, T. Jonas, and A. Wüest. 2002. Dynamics of turbulence in low-speed oscillating bottom-boundary layers of stratified basins. Environ. Fluid Mech. 2:291-313 [doi:10.1023/A:1020450729821].

———, B. Muller, M. Maerki, and A. Wuest. 2003. Breathing sediments: The control of diffusive transport across the sediment-water interface by periodic boundary-layer turbulence. Limnol. Oceanogr. 48:2077-2085 [doi:10.4319/lo.2003.48.6.2077].

———, L. Umlauf, and V. Mohrholz. 2008. Stratification and mixing on sloping boundaries. Geophys. Res. Lett. 35, L14610, 5PP [doi:10.1029/2008GL034607].

McGinnis, D. F., P. Berg, A. Brand, C. Lorrai, T. J. Edmonds, and A. Wüest. 2008. Measurements of eddy correlation oxygen fluxes in shallow freshwaters: Towards routine applications and analysis. Geophys. Res. Lett. 35, L04403, 5 PP [doi:10.1029/2007GL032747].

Nielsen, L. P. 1992. Denitrification in sediment determined from nitrogen isotope pairing. FEMS Microbiol. Ecol. 86:357-362 [doi:10.1111/j.1574-6968.1992.tb04828.x].

Pope, S. B. 2000. Turbulent flows. Cambridge Univ. Press.

Ritzrau, W. 1996. Microbial activity in the benthic boundary layer: Small-scale distribution and its relationship to the hydrodynamic regime. J. Sea Res. 36:171-180 [doi:10.1016/S1385-1101(96)90787-X].

Rysgaard, S., H. Fossing, and M. M. Jensen. 2001. Organic matter degradation through oxygen respiration, denitrification, and manganese, iron, and sulfate reduction in marine sediments (the Kattegat and the Skagerrak). Ophelia 55:77-91.

Sauter, E. J., M. Schluter, J. Wegner, and E. Labahn. 2005. A routine device for high resolution bottom water sampling. J. Sea Res. 54:204-210 [doi:10.1016/j.seares.2005.04.005].

Schulz, H. D. 2000. Quantification of early diagenisis: dissolved constituents in marine pore water, p. 85-128. *In* H. D. Schulz and M. Zabel [eds.], Marine geochemistry. Springer.

Seeberg-Elverfeldt, J., M. Schlueter, T. Feseker, and M. Kolling. 2005. Rhizon sampling of porewaters near the sediment-water interface of aquatic systems. Limnol. Oceanogr. Methods 3:361-371.

Soetaert, K., J. J. Middelburg, P. M. J. Herman, and K. Buis. 2000. On the coupling of benthic and pelagic biogeochemical models. Earth Sci. Rev. 51:173-201 [doi:10.1016/S0012-8252(00)00004-0].

Tengberg, A., and others. 2005. Intercalibration of benthic flux chambers II. Hydrodynamic characterization and flux comparisons of 14 different designs. Mar. Chem. 94:147-173 [doi:10.1016/j.marchem.2004.07.014].

Tennekes, H., and J. L. Lumley. 1972. A first course in turbulence. MIT Press.

Thamdrup, B., and D. Canfield. 2000. Benthic respiration in aquatic sediments, p. 86-103. *In* O. Sala, H. Mooney, R. Jackson, and R. Howarth [eds.], Methods in ecosystem science. Springer.

Thomsen, L., and G. Graf. 1994. Boundary-layer characteristics of the continental-margin of the Western Barents Sea. Oceanolog. Acta 17:597-607.

von Kármán, T. 1930. Mechanische Ähnlichkeit und Turbu-

lenz, p. 85-105. *In* Proceedings of the Third International Congress of Applied Mechanics, Vol 1, Norstedt and Sons, Stockholm.

Wenzhoefer, F., O. Holby, and O. Kohls. 2001. Deep penetrating benthic oxygen profiles measured in situ by oxygen optodes. Deep Sea Res. I 48:1741-1755 [doi:10.1016/S0967-0637(00)00108-4].

Wilczak, J., S. Oncley, and S. Stage. 2001. Sonic anemometer tilt correction algorithms. Bound. Layer Meteorol. 99:127-150 [doi:10.1023/A:1018966204465].

Wollast, R. 1991. The coastal organic carbon cycle: fluxes, sources and sinks, p. 365-381. *In* J.M.M.R.F.C. Mantoura and R. Wollast [ed.], Ocean margin processes in global change. John Wiley & Sons.

Submitted 8 April 2010
Revised 3 November 2010
Accepted 6 December 2010